



Development And Application of WRF (v4.1.2)-uEMEP(v5) Model at the City with the Highest Industrial Density: A Case Study of Foshan

Liting Yang¹, Ming Chang^{1,*}, Shuping Situ², Weiwen Wang¹, Xuemei Wang¹

¹Guangdong-Hongkong-Macau Joint Laboratory of Collaborative Innovation for Environmental
5 Quality, Institute for Environmental and Climate Research, Jinan University, Guangzhou, 511443,
China

²Foshan Ecological and Environmental Monitoring Station of Guangdong Province, Foshan, 528000,
China

Correspondence to: Ming Chang (changming@email.jnu.edu.cn)

10 Abstract.

The study aims to develop and apply the WRF-uEMEP model to simulate air quality at the city scale,
with a focus on Foshan, the city with the highest industrial density. The interaction between
atmospheric diffusion and chemical reactions in different regions further complicates the modeling
process. Therefore, this study proposes a multi-scale approach to build an urban air quality model with a
15 resolution of 250 meters by integrating different models. The model takes into account the effects of
urban structure and takes into account atmospheric diffusion and chemical reactions in different regions.
The research process included model development, calibration, and validation using existing air quality
data in Foshan. The study shows that the WRF-uEMEP model effectively captures the impact of urban
structure on air pollutant processes. The simulation results reveal the spatial and temporal distribution of
20 air pollutants in Foshan, providing valuable insights for urban air quality management.

1 Introduction

Due to the limitations of traditional ground-based observations on spatial and temporal scales, the study
of regional air quality is mostly carried out with the help of numerical models. At present, there is very
25 little model that can meet all the requirements of urban air quality management, and the air quality
model at the regional/city scale can reflect the degree of influence of urban structure (building volume
and road network, etc.) on physical and chemical processes such as the transport, transformation and
deposition of air pollutants, but it also needs to take into account the interaction of atmospheric
diffusion and chemical reactions between regions/countries and regions/countries, so the establishment
30 of urban air quality models at the scale of 100 meters requires the combination of different scale
models (Anjali and Rao, 2011; Chen et al., 2011).

At present, multi-scale air quality models have been applied in many urban areas to meet the needs of
urban air quality management. The Enviro-HIRLAM-M2UE model was tested for multi-scale air
pollution and emergency protection in the Copenhagen region of Denmark, and the results of the single-

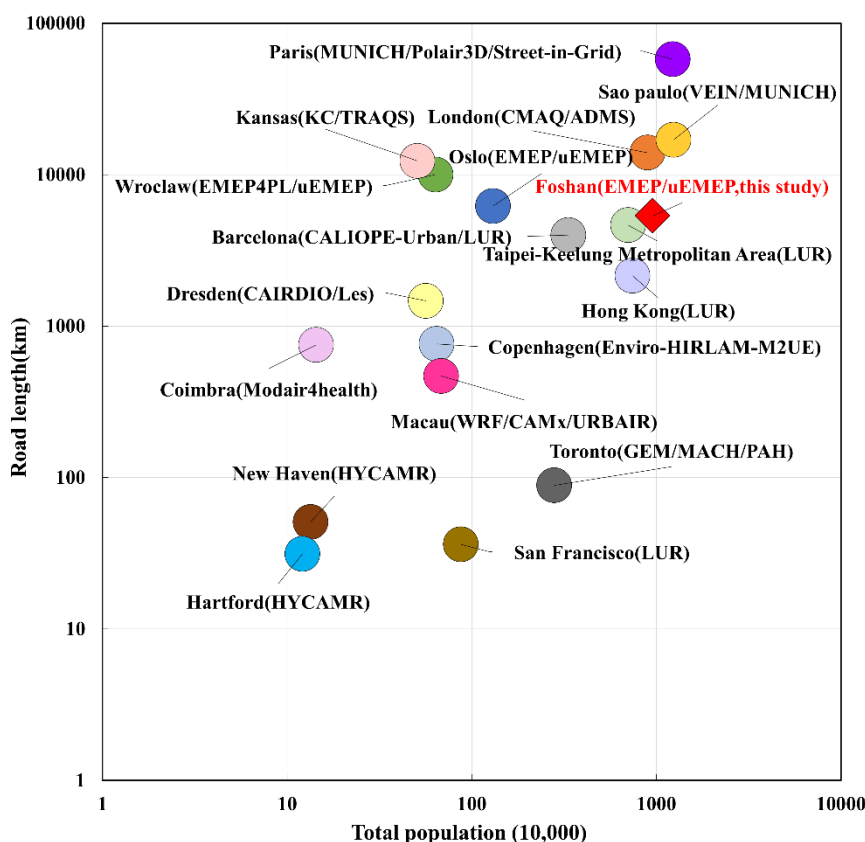


35 layer nested multi-scale model were satisfactory, but the resolution of the microscale model was
recommended to be 3-5 times higher than that of the previous model(Baklanov and Nuterman, 2009).
CMAQ-ADMS(Roads) uses WRF to input the meteorological field to CMAQ, and the CMAQ
simulation grid is reduced to 20 meters by bilinear interpolation, and then combined with the ADMS
40 (Roads) model to simulate the nitrogen oxide concentration on the roads in London, England, but there
is a certain error in the location of the model simulation close to the road(Beevers et al., 2012). Street-
in-Grid (SinG) combines a street network model, an urban network model of cross-canyons and roads
(MUNICH) and a chemical transport model Polair3D to simulate the concentration of nitrogen oxides in
the suburbs of Paris, but the new model fails to demonstrate the ability to assess background
concentrations compared to traditional chemical transport models(Kim et al., 2018). The Modair4health
45 system, which includes the online model WRF-Chem and the fluid mechanics model VADIS, uses
linear and nonlinear methods to calculate morbidity and mortality in order to quantify the health effects
of air pollution, and is an important multi-scale model tool for comprehensive air quality and health
assessment in the city of Coimbra, Portugal (Silveira et al., 2023). KC-TRAQS combines the diffusion
model and local air quality measurement datasets to estimate the relative contribution of air pollution in
50 Kansas City, USA(Isakov et al., 2019), and similarly, following the processing and analysis of feasible
data procedures, the LUR method is applied in many countries and cities, such as Hong Kong, Taipei-
Keelung Metropolitan Area, Barcelona, Spain, and San Francisco, USA, but can only reflect the air
pollution during the period of use (Bai et al., 2023; Criado et al., 2022; Li et al., 2021; Li et al., 2023).
The GEM-MACH-PAH was used in Toronto, Canada, to explore the contribution of motor vehicles to
55 benzene and polycyclic aromatic hydrocarbons in ambient air, but the uncertainty of atmospheric
chemistry is difficult to assess(Whaley et al., 2020). HYCAMR combines the community model CAMx
and the block-scale diffusion model R-LINE to estimate pollutant concentrations in the near-road
environment, but does not take into account the emission factors of different roads(Parvez and
Wagstrom, 2019). The CAIRDIO-Les large vortex model simulates micrometeorology and air pollution
60 in the Dresden Basin, Germany(Weger and Heinold, 2023). The VEIN-MUNICH model was developed
and applied to the road-dense city of São Paulo, Brazil, to predict NOx emissions from road
vehicles(Gavidia-Calderón et al., 2021). Multi-scale air quality models have been effectively developed
and applied in urban air quality management, and can increasingly meet the requirements of urban air
quality management.

65 The uEMEP model is based on the well-known Gaussian principle, and the uniqueness of the model lies
in the fact that it performs the "local fraction" calculation included in the EMEP model, which allows
the uEMEP model to be embedded in the EMEP model, making the model suitable for high-resolution
calculations, and the uEMEP model has been successfully applied in Norway, Poland and other
countries and regions(Maciej Kryza, 2022; Denby et al., 2020). Located in the Pearl River Delta region
70 of Guangdong Province, Foshan is an important component city of the Guangdong-Hong Kong-Macao
Greater Bay Area, a typical manufacturing city in the developed coastal areas of southern China, and
was once known as the manufacturing capital of the world(Liu et al., 2023). Figure 1 reveal that,
compared with the above-mentioned countries/regions that have applied the 100-meter-scale urban air
quality model, Foshan is in a period of rapid urbanization and industrialization, due to its high
75 population density and complex road network, and the complex urban building structure and large
number of motor vehicle exhaust emissions have made the air quality in Foshan an unprecedented



challenge. Therefore, this study intends to use the mesoscale meteorological model WRF combined with the air quality downscaling model uEMEP to achieve high-resolution air quality modeling at the block scale in Foshan City, and to better understand the performance of the 100-meter scale numerical
80 model. It helps people to grasp the air pollution situation in urban areas more accurately, so as to put forward more scientific and targeted action plans to alleviate air pollution.



85 Figure 1: Urban population and road network conditions using street resolution prediction models.

2 Methodology

2.1 The WRF-EMEP-uEMEP model description

In this study, the regional weather prediction model WRF (v4.1.2), the chemical transport model EMEP (rv4_33) and the downscaling chemical transport model uEMEP (v5) were used to simulate the spatial and temporal distributions of nitrogen oxides, particulate matter and ozone concentrations in Foshan. As
90 shown in Fig. 2(a), the WRF model covers the entire Pearl River Delta with two layers of nesting, the number of simulated grids is set to 130×110, 136×151, the horizontal grid resolution is 9km×9km, 3km×3km, the model top pressure is set to 100 hPa, and the vertical direction is divided into 30 layers.



As shown in Fig. 2(b), the study area, mesh number, and mesh resolution of the EMEP model are the same as those of the second layer of the WRF model. As shown in Fig. 2(c), the mesh range of the uEMEP model covers the city of Foshan, and the number of simulated meshes is set to 480×480 and the horizontal resolution is 250m×250m.

The WRF model weather field is driven by global 1°×1° reanalysis data (http://rda.ucar.edu/datasets/ds083.2/, FNL) and the land use information uses data GLC2020 the European Space Agency (ESA). Table 1 shows the physical parameterization and chemical protocols of WRF-EMEP-uEMEP.

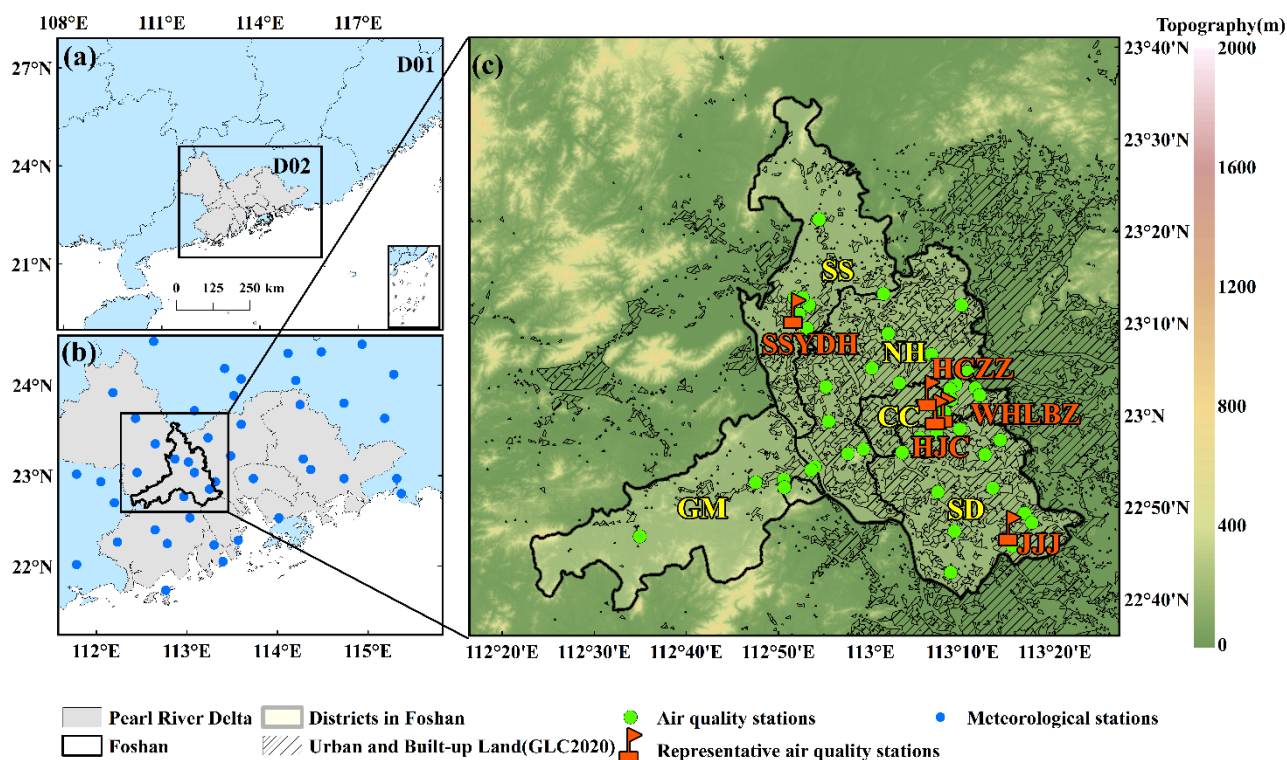


Figure 2: Model domains and locations of 33 air quality monitoring stations (green dots), 47 meteorological stations (blue dots), and 5 representative air quality monitoring stations (red flags). The figure on the right shows the elevation of the terrain (m). The 5 representative air quality monitoring stations are Sanshuiyundonghai (SSYDH, suburban station), Jinjiju (JJJ, industrial station), Huacaizhizhong (HCZZ, urban-developed station), Huijingcheng (HJC, urban-developing station), and Wenhualubianzhan (WHLBZ, roadside station). The 5 districts in Foshan are Sanshui district(SS), Nanhai district(NH), Chancheng district(CC), Gaoming district(GM), and Shunde district(SD). (a) WRF mode domain settings; (b) EMEP mode domain settings; (c) uEMEP mode domain settings.

Table 1: WRF-EMEP-uEMEP simulation physical and chemical parameterization scheme settings.

Scheme	Processes	Parameterization
Physical	Microphysics	Morrison double-moment



	Longwave Radiation	RRTMG scheme
	Shortwave Radiation	RRTMG shortwave
	Surface Layer	Eta similarity
	Land Surface	Noah-MP Land Surface Model
	Urban Surface	BEM
	Planetary Boundary layer	Mellor-Yamada-Janjic scheme
	Cumulus Parameterization	Grell-3
Chemical	Chemism	EmChem09

2.2 Introduction to uEMEP downscaling methods

115 The uEMEP mode can be run using two downscaling methods, both of which utilize a Gaussian
 diffusion model to simulate the concentration of contaminants at high resolution. The choice of
 downscaling method will depend on high-resolution emissions data, the first of which is the emissions
 redistribution method, which means that only the following types of high-resolution emissions data are
 available, such as population density, road network data, or land-use data. The second downscaling
 120 method, the independent emission method, is available in both uEMEP and EMEP modes of input high
 spatiotemporal resolution emission inventories, and the gridded emissions data are fully consistent with
 the local emissions data, i.e., the proxy data is given in the form of emissions and summarized into the
 CTM grid emissions, and the two methods are equivalent (Mu et al., 2022). Based on the emission
 redistribution method, the EMEP-uEMEP model can be used to simulate the air quality at the scale of
 125 100-meter urban blocks, and effectively simulate the diffusion of ozone precursors and particulate
 matter at the scale of urban blocks, which has broad application prospects.

2.3 The Development methods for localized emissions inventories

In order to accurately simulate air quality at multiple scales, it is necessary not only to ensure that the
 boundary layer conditions and background meteorological environment and other relevant variables in
 130 the local scale air quality model can be accurately identified by the microscale model, but also to
 respond to multiple scale emission inventories and other required multi-scale inventories (Russo et al.,
 2019). The production of localized multi-scale emission inventories often requires a lot of manpower
 and material resources, and it is difficult to carry out large-scale investigation and production. Due to
 the difficulty of localizing the preparation and preparation of the list, it is difficult to deploy and apply
 135 the block-scale model in China.

All input files required for the EMEP model (except aircraft emissions data and forest fire emission
 data) can be downloaded from the EMEP open source website, including land use data, road dust data,
 emission source data, time allocation factor data, settlement data, etc. (Simpson et al., 2012). However,
 the original land use data and emission data provided by the EMEP model are only applicable to the
 140 European region, so the land use data and emission source data need to be updated locally. In this study,
 the 2017 China Monthly Average Multi-Resolution Emissions Inventory
 (<http://meicmodel.org.cn>, MEIC) data was used to replace the European emission source data in EMEP.



The SNAP classification method is used to input the emission inventory in the EMEP model, and the pollution source types in the MEIC 2017 emission data are divided into five categories: fixed
145 combustion sources, residential sources, industrial sources, transportation sources, and agricultural sources. The formula for converting a MEIC list to a SNAP list is as follows Eq. (1):

$$E_o^i = \sum_1^J (E_o^j \times f_o^j) \quad (1)$$

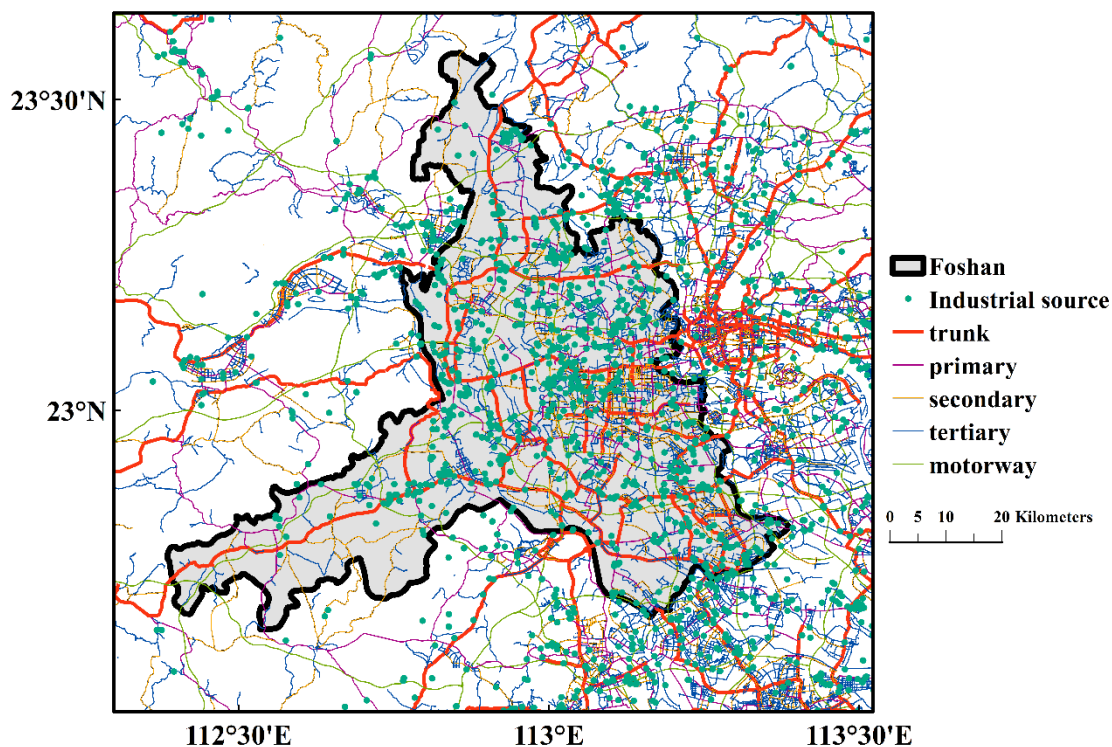
where $o=1,2,\dots,O$; O is the pollutant type; $i=1,2,\dots,I$; I is the number of SNAP classifications; $j=1,2,\dots,J$; J
150 is the MEIC classification number; E_o^j is the amount of each pollutant in the MEIC inventory; f_o^j is the allocation coefficient of each pollutant in the MEIC inventory; and E_o^i is the SNAP classification benchmark of each pollutant.

The formula for calculating pollutants in the EMEP model is as follows Eq. (2):

$$E_t^i = E_o^i \times f_{m.PRD}^i \times f_{h.PRD}^i \quad (2)$$

where $i=1, 2, \dots, I$; I is the number of SNAP classifications; t is a certain time; $f_{m.PRD}^i$ is the local
155 monthly time allocation factor in the Pearl River Delta; $f_{h.PRD}^i$ is the local hourly time allocation factor in the Pearl River Delta; E_t^i is the calculated amount of pollutants.

The main types of emission data that need to be prepared for uEMEP are: road mobile sources, industrial point sources, shipping emission sources and residential sources. For the preparation of Foshan's local emission data, this study uses OpenStreetMap (OSM)(Openstreetmap Contributors,
160 2020) road network data, uses localized road weights to obtain traffic exhaust emission data, and uses the Global Human Settlement Layer (<http://data.europa.eu/89h/2ff68a52-5b5b-4a22-8f40-c41da8332cfe>) 250m grid population data replaces the residential wood burning emission data, the localized shipping emission data of the Pearl River Delta is used, and the shipping emission data is NOx emissions, covering the main rivers and shipping ports of the Pearl River Delta, and the industrial point source emission data of Foshan is used to reduce the emission data of NOx and particulate matter(Fig.
165 3).



170 **Figure 3: Spatial distribution of road network and industrial point sources in Foshan, China. Road network map :
©OpenStreetMap, distributed under the Open Data Commons Open Database License (ODbL) v1.0.**

2.4 Measurement Datasets

The meteorological observation data used in this study are the hourly observation data of China's surface weather stations in the Pearl River Delta in 2021 (<https://data.cma.cn/>), with a total of 47
175 meteorological stations, and the mesoscale and block-scale pollutant data are based on the conventional pollutant observation data of the Guangdong Air Quality Forecasting and Early Warning Center (<http://113.108.142.147:20032/Home/Index>), with a total of 38 ambient air quality monitoring stations. The distribution of meteorological and ambient air quality monitoring stations is shown in Fig. 2.

2.5 Case classification

180 In this study, the only four NO₂ pollution cases in Foshan in 2021 were subjectively classified by weather patterns and simulation experiments were carried out (Yan et al., 2021). The L1 period is January 13, 2021 - January 16, 2021 Beijing time, during which NO₂ and PM_{2.5} are combined pollution, and the weather situation is high-pressure control and frontal influence. The L2 period is January 19, 2021 ~ January 20, 2021 Beijing time, and the weather period is NO₂ pollution, and the weather
185 situation is high-pressure out-of-sea type and high-pressure control type. The L3 period is December 11,



2021 Beijing time, during which NO₂ pollution is carried out and the weather situation is high-pressure controlled. The L4 period is December 15, 2021 Beijing time, during which NO₂ pollution and the weather situation is high-pressure out of the sea (Table 2). The simulation performance of uEMEP is reflected by simulating the pollution of NO₂ under different weather patterns, and the simulation performance evaluation formula is detailed in Appendix A.

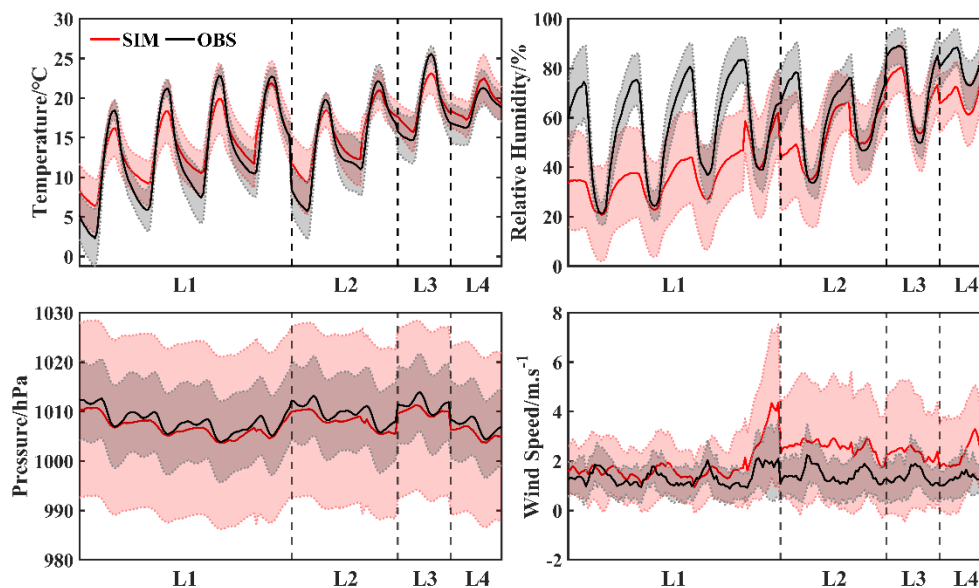
Table 2: Case classification.

Case number	Case type	Weather type	Date	Primary contaminant	Concentration ($\mu\text{g m}^{-3}$)
L1	Compound pollution	High pressure control + front impact	2021/1/13	NO ₂	88
			2021/1/14	PM _{2.5}	101
			2021/1/15	NO ₂	137
			2021/1/16	PM _{2.5}	116
L2	Pollution incidents	High-pressure going to sea + high-pressure control	2021/1/19	NO ₂	87
			2021/1/20		125
L3	Single contamination	High voltage control	2021/12/11	NO ₂	82
L4		High-pressure access to the sea	2021/12/15	NO ₂	88

3 Results

3.1 Evaluation of the meteorological simulation performance

In order to verify the simulation ability and reliability of the model, the observed data and the simulated data were used to compare and verify, which are detailed in Appendix A. As can be seen from Table B1 of Appendix B, the 2m temperature simulation for the L2 case is slightly overestimated ($0.6\text{ K} > \pm 0.5\text{ K}$), but the *IOA* is compliant ($IOA \geq 0.8$), and the 2m temperature simulation for L1, L3, and L4 simulations are all compliant. The L1 simulated relative humidity has a deviation of -1.6 g kg^{-1} , but the *IOA* meets the standard ($IOA \geq 0.6$). There is a certain deviation (0.5, 0.4, 0.1) in the *IOA* of L2, L3 and L4 simulations, but the comparison of the relative humidity of the three pollution periods shows that there is a significant correlation (0.7-0.8) between the hourly observed values and the simulated values, which indicates the rationality of the simulation. In terms of wind speed, although the *R* is not high and the *MB* is somewhat overestimated ($> \pm 0.5\text{ m s}^{-1}$), both *RMSE* and *IOA* are within the standard range ($RMSE \leq 2.0\text{ m/s}$, $IOA \geq 0.6$). In addition, the temporal series changes of meteorological conditions are analyzed, and the model performance can reproduce the temporal and spatial changes of meteorological conditions well (Fig. 4). Therefore, the WRF model is reliable for meteorological results for the four pollution periods.



210

Figure 4: Shadow plots of simulation and observed error in 4 cases, where the shaded part represents the standard deviation.

3.2 Evaluation of the air quality simulation performance

As can be seen from Table B2 ~ Table B5 of Appendix B, the NME of NO₂ and PM_{2.5} in the four cases simulated by EMEP reached the standard (NO₂:NME<80%, PM_{2.5}:NME<150%), the NME of NO₂ and PM_{2.5} in the L1, L2 and L3 cases simulated by uEMEP reached the standard (NO₂:NME<80%, PM_{2.5}:NME<150%), the R of NO₂ and PM_{2.5} simulated by EMEP reached the standard (0.3~0.6, 0.4~0.5), and the R of L2 and L4 simulated by uEMEP reached the standard (0.3~0.6, 0.3~0.4), the R of O₃ simulated by EMEP and uEMEP reached the standard (R>0.4), and there was a strong correlation (0.6~0.9). Comparing the simulation performance of EMEP and uEMEP models, it is found that for NO₂ and L4, uEMEP simulation performance is better, but for other cases, the standard deviation and correlation coefficient of uEMEP simulation O₃ in four cases are better than those of EMEP model, for PM_{2.5}, the simulation performance of uEMEP in L4 is better, but the simulation performance of uEMEP in other cases is poor, for PM₁₀, L1, L2, The EMEP simulation performance is better in L3 and the uEMEP simulation performance is better in L1 (Fig. 5).

In general, the performance of the uEMEP model in the L1 case is weaker than that of the EMEP model, the simulation of uEMEP for NO₂, O₃ and PM₁₀ in the L2 case is better than EMEP, the simulation of uEMEP for O₃, PM_{2.5} and PM₁₀ in the L3 case is better than that of EMEP, and the simulation of uEMEP for O₃ and PM₁₀ in the L4 case is better than that of EMEP. The overall simulation deviation of uEMEP is large, NO₂ is between -95%~-58%, O₃ is between -57%~33%, PM_{2.5} is between -92%~-70%, and PM₁₀ is between -93%~-76%.

225
230

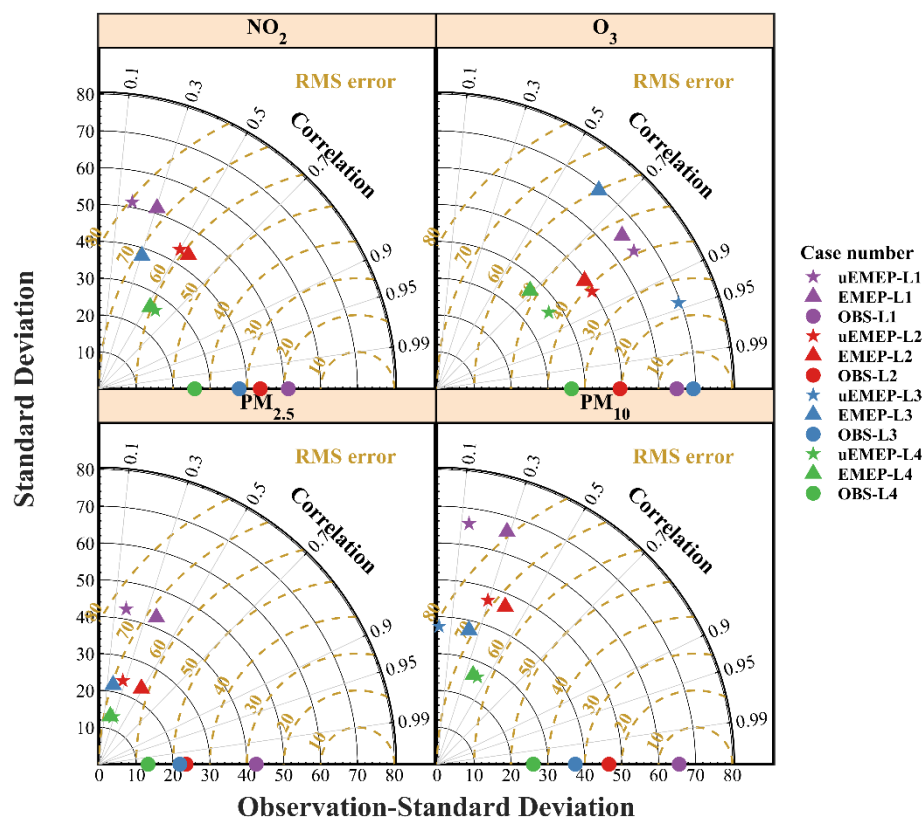


Figure 5: Comparison of NO₂, O₃, PM_{2.5} and PM₁₀ between EMEP and uEMEP models.

3.3 Spatial characteristics of air pollution

In case L1, From January 13 to January 16, 2021, a compound pollution event occurred in Foshan
 City, with the high-pressure control type as the dominant weather type and the frontal influence type as
 the secondary weather type. The daily average concentrations of NO₂ and PM_{2.5} reached 88-137 μg m⁻³
 and 101-116 μg m⁻³, respectively (Table 2).

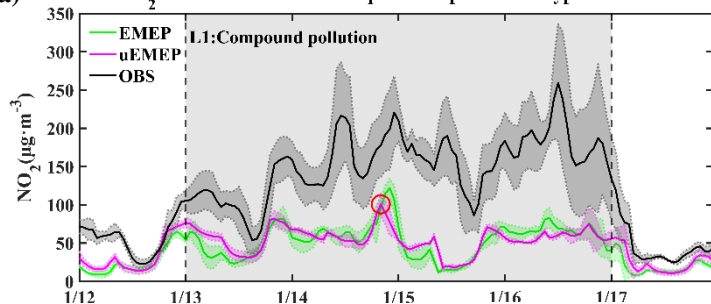
From January 13th to January 15th, the high-altitude and low-altitude circulation configuration under
 the control of high pressure caused the vertical stratification of the atmosphere to tend to be stable, and
 the low temperature and low humidity conditions are not conducive to the photochemical conversion of
 NO₂. On January 16, the weather conditions of the front caused the air in front of the cold front to
 accumulate air, and the convergence of the wind field hindered the upward diffusion and outward
 transport of local pollutants in Foshan. The spatial distribution of NO₂ follows the road network setting.
 The high value of NO₂ occurred at 20:00 on January 14 (Fig. 6(a)), and the high value area of NO₂ was
 S263 and S81 in Nanhai District, Guangzhou-Foshan junction in the northeast of Foshan City(Fig. 6(b)-
 Fig. 6(c)). From the evening of January 14 (19:00-23:00) to the early morning of January 15 (00:00-
 08:00), a large amount of NO₂ was accumulated, and the traffic pressure in Foshan during the morning
 and evening rush hours was high, resulting in NO₂ pollution on January 15.



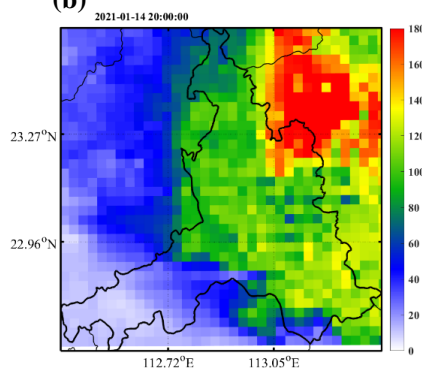
250 NO₂ is the primary pollutant in the early stage of the pollution process, and the enhancement of
atmospheric oxidation is one of the reasons for the increase of PM_{2.5} concentration. The spatial
distribution of PM_{2.5} pollution is mainly affected by industrial point sources, followed by road network
settings. The high PM_{2.5} value occurred at 12:00 on January 16(Fig. 6(d)), and the wind speed was small
during the day, which was not conducive to the diffusion of high-concentration PM_{2.5} industrial point
sources, resulting in local accumulation of PM_{2.5}(Fig. 6(e)- Fig. 6(f)). On January 14, the convergence
255 of wind fields during the day was not conducive to the spread of PM_{2.5}, and PM_{2.5} continued to
accumulate, resulting in PM_{2.5} pollution.
The composite pollution event was mainly affected by meteorological conditions, and regional
transmission accounted for a large proportion. At the same time, Foshan's local industries gradually
began to resume production and work in January(Foshan Emergency Management Bureau and Office,
260 2021), resulting in an increase in local emissions, resulting in a combined NO₂ and PM_{2.5} pollution
incident.



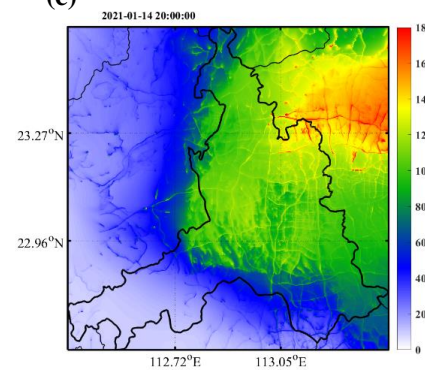
(a) NO_2 simulation results of L1 pollution period at 5 typical stations



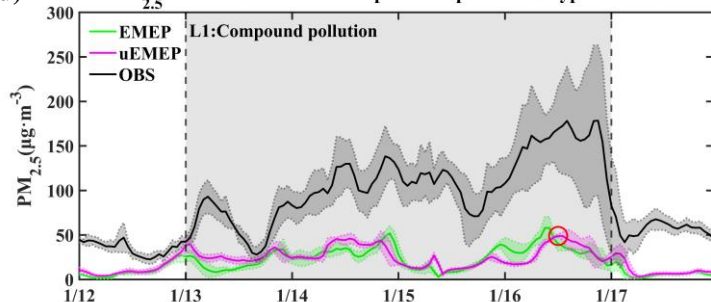
(b)



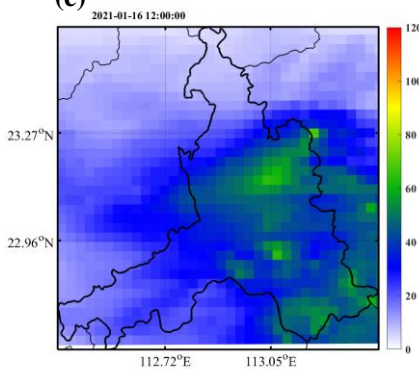
(c)



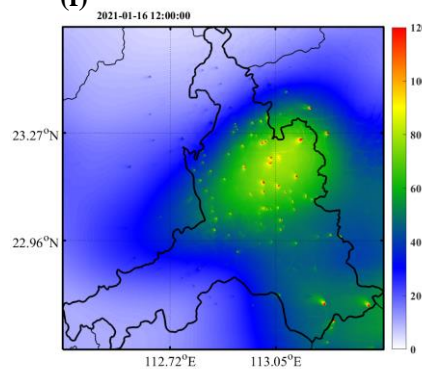
(d) $\text{PM}_{2.5}$ simulation results of L1 pollution period at 5 typical stations



(e)



(f)





265

270

Figure 6: The time series simulation results of NO₂ and PM_{2.5}, and spatial distribution of uEMEP simulation at the peak moment (red hollow circle) in L1 case. (a): Time series of NO₂ simulation results (shaded part is the standard deviation of 5 typical stations). (b) Spatial distribution of NO₂ simulated by EMEP at 20:00 on January 14, 2021. (c) Spatial distribution of NO₂ simulated by uEMEP at 20:00 on January 14, 2021. (d) Time series of PM_{2.5} simulation results (shaded part is the standard deviation of 5 typical stations). (e) Spatial distribution of PM_{2.5} simulated by EMEP at 20:00 on January 14, 2021. (f) Spatial distribution of PM_{2.5} simulated by uEMEP at 20:00 on January 14, 2021.

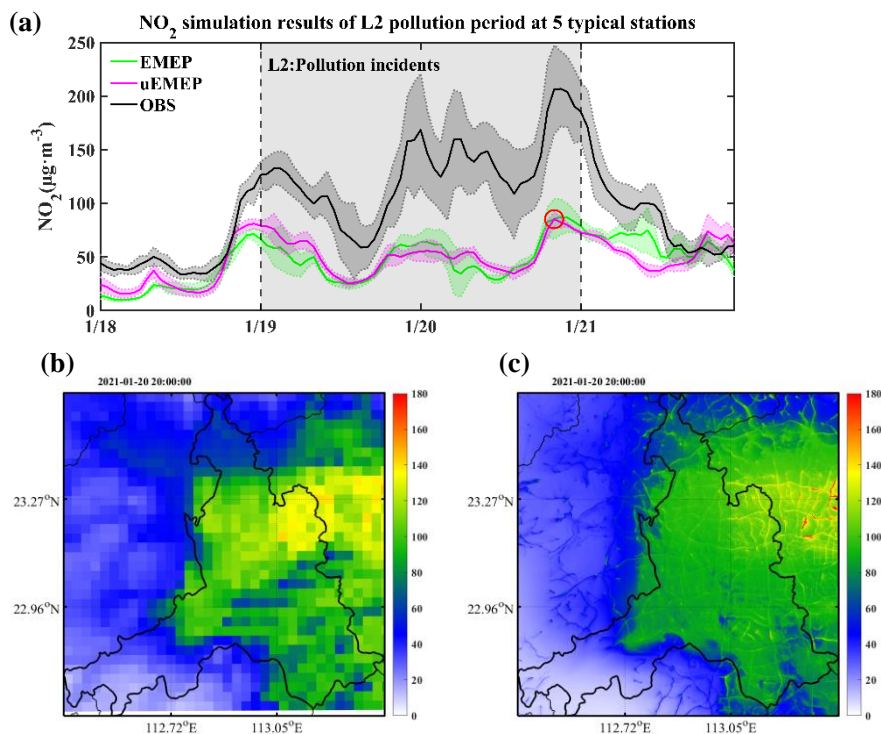
275

280

285

In case L2, continuous NO₂ pollution occurred on January 19, 2021 and January 20, 2021 in Foshan City under the combined action of high-pressure controlled weather and high-pressure sea-moving weather. The average daily concentration of NO₂ reached 87-125 $\mu\text{g m}^{-3}$ (Table 2). The spatial distribution of NO₂ follows the road network setting. The high value of NO₂ occurred at 20:00 on January 20 (Fig. 7(a)), and the high value of NO₂ was in the Sanshui District and Nanhai District in the north of Foshan City, and the traffic pressure was greater (Fig. 7(b)- Fig. 7(c)). The ventilation coefficient was small under the high-pressure weather conditions on January 19, and the near-surface pressure gradient decreased and the wind speed weakened under the high-pressure controlled weather conditions on January 20, which was not conducive to the horizontal transportation of air pollutants and hindered the upward and outward transmission of local pollutants in Foshan City.

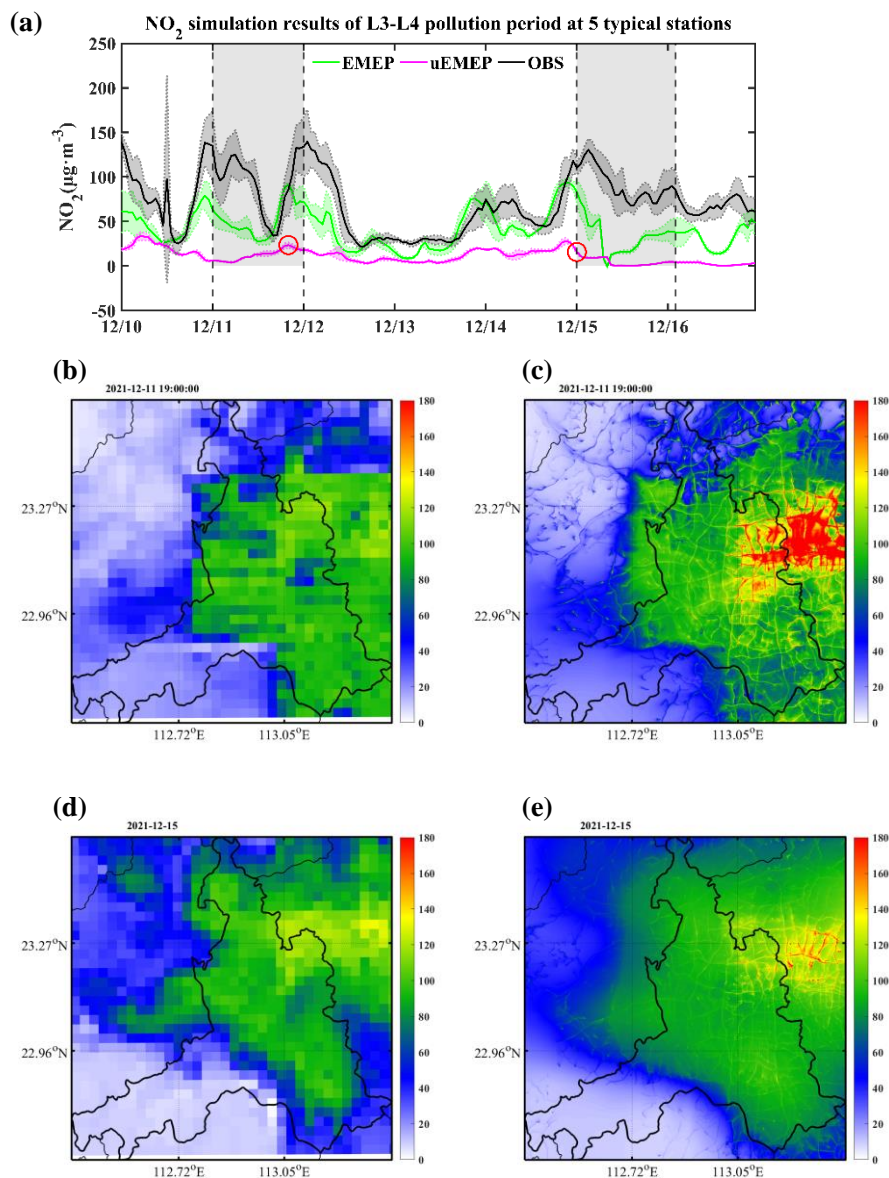
This compound pollution event is mainly affected by meteorological conditions, and the turbulence is weak, which is not conducive to the horizontal transport of air pollutants and hinders the upward and outward transmission. At the same time, Foshan's local industries gradually began to resume production and work in January, resulting in an increase in local emissions, resulting in a continuous NO₂ pollution incident.



290 **Figure 7: The time series simulation results of NO₂, and spatial distribution of uEMEP simulation at the peak moment (red hollow circle) in L2 case. (a): Time series of NO₂ simulation results (shaded part is the standard deviation of 5 typical stations). (b) Spatial distribution of NO₂ simulated by EMEP at 20:00 on January 20, 2021. (c) Spatial distribution of NO₂ simulated by uEMEP at 20:00 on January 20, 2021.**

In case L3, on December 11, 2021, a NO₂ pollution occurred in Foshan City with high pressure control as the dominant weather. The average daily concentration of NO₂ reached 82 µg m⁻³ (Table 2). The high value of NO₂ occurred at 19:00 on December 11 (Fig. 8(a)), and the high value of NO₂ was concentrated in the S81 and S55 areas at the junction of Guangzhou-Foshan in the central and eastern part of Foshan City (Fig. 8(b)- Fig. 8(c)), and the traffic pressure was greater. Under the high-pressure controlled weather conditions on December 11, the pressure gradient near the surface decreased, and the wind speed weakened, which was not conducive to the migration and dispersion of pollutants. At the same time, the density of local vehicles in Foshan City increased during the morning and evening rush hours, which intensified the traffic pressure and caused the pollution incident.

300 In case L4, On December 15, 2021, a NO₂ pollution occurred in Foshan City, where high pressure was the dominant weather. The average daily concentration of NO₂ reached 88 µg m⁻³ (Table 2). The high value of NO₂ occurred at 00:00 on December 15 (Fig. 8(a)), and the high value of NO₂ was concentrated in the S81 and S55 areas at the junction of Guangzhou-Foshan in the central and eastern part of Foshan City (Fig. 8(d)- Fig. 8(e)). On December 15, the ventilation coefficient was small and the wind speed weakened, which hindered the upward diffusion and outward transport of local pollutants in Foshan, and the NO₂ concentration continued to accumulate on the night of the 14th (20:00-23:00), triggering a pollution incident.



310

Figure 8: The time series simulation results of NO₂, and spatial distribution of uEMEP simulation at the peak moment (red hollow circle) in L3 and L4 case. (a): Time series of NO₂ simulation results (shaded part is the standard deviation of 5 typical stations). (b) Spatial distribution of NO₂ simulated by EMEP at 20:00 on December 11, 2021. (c) Spatial distribution of NO₂ simulated by uEMEP at 20:00 on December 11, 2021. (d) Spatial distribution of NO₂ simulated by EMEP at 00:00 on December 15, 2021. (e) Spatial distribution of NO₂ simulated by uEMEP at 00:00 on December 15, 2021.

315

Combined with the analysis of the weather circulation situation, compared with the high-pressure weather pattern of L2 and L4 with relatively quiet and small winds, we find that L1 and L3 are sudden and transient weather patterns, especially in the late stage of L1, there is a cold front transit, and the

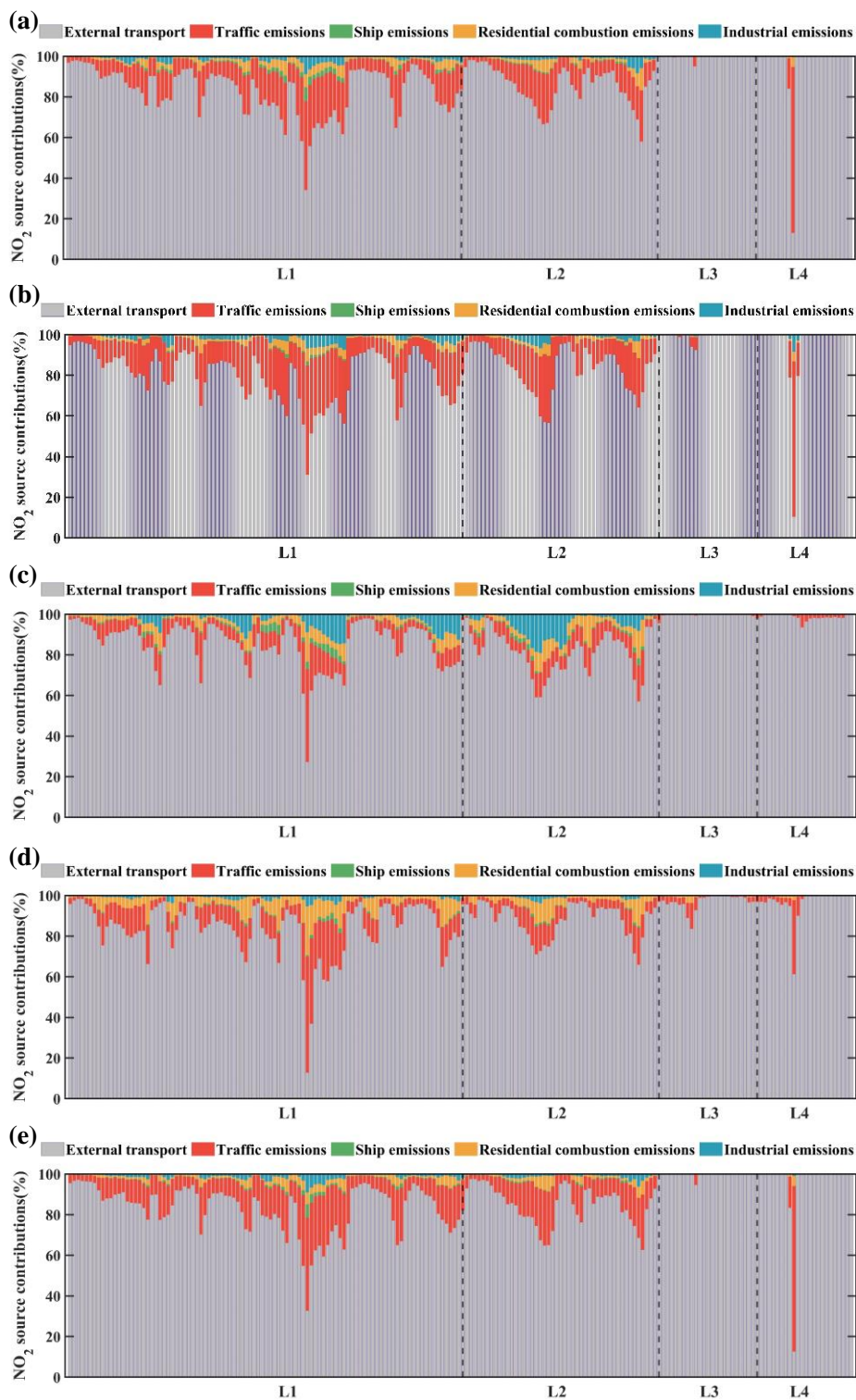


320 meteorological elements suddenly change, and the $PM_{2.5}$ concentration near the surface rises through regional transmission, but the WRF meteorological model is difficult to capture the sudden turbulence phenomenon, which makes the meteorological field input to the EMEP model have great uncertainty, and at the same time, it is difficult for uEMEP to restore the pollutant diffusion phenomenon caused by sudden weather phenomena based on the Gaussian plume principle, so the uEMEP simulation performance of L1 and L3 is poor.

325 After the fine simulation deployment with high spatiotemporal resolution in Foshan, comparing the spatial distribution of NO_2 between the EMEP model and the uEMEP model, it can be seen that the application of the block scale in Foshan can more accurately simulate the distribution and change of air pollutant concentration, and put forward more scientific and targeted action plans to alleviate air pollution.

330 3.4 Analysis of NO_2 traceability characteristics

In order to quantitatively analyze the sources of NO_2 pollution in four cases in different local areas of Foshan City, and identify the sources of pollutants affecting the ambient air quality monitoring stations in each city, Sanshuiyundonghai (SSYDH, suburban station), Jinjiju (JJJ, industrial station), Huacaizhizhong (HCZZ, urban-developed station), Huijingcheng (HJC, urban-developing station), and
335 Wenhualubianzhan (WHLBZ, roadside station) were selected for analysis (Ecological and Environmental Monitoring Centre of Guangdong et al., 2023; Liu et al., 2011). The two urban stations (HJC, HCZZ) are located in the center of Chancheng District, Foshan City, and are affected by multiple pollution sources such as traffic, industry and residents. Comparing the two urban sites, we find that the average proportions of HJC regional transmission, shipping emissions and
340 industrial emissions in these four cases are 87.3%, 1.6% and 0.6%, respectively, which is slightly larger than that of HCZZ (85%, 1.4% and 0.2%), and the average proportion of HJC industrial emissions in case L1 reaches 1%, which is greater than that of HCZZ (0.3%). JJJ is located in Shunde District, the concentration level of high-tech enterprises is higher than the overall level of Foshan City and continues to grow (Bo et al., 2023), its average shipping emissions account for 2.6%, industrial emissions account
345 for 0.8%, and residential emissions account for 3%, and the average proportion of JJJ industrial emissions in case L1 is 1.1%, and the proportion of residential emissions is 3.3%, which is larger than the other four stations. SSYDH is located in Sanshui District, which is a representative station in the suburbs, and its average proportion of shipping emissions is 3.6%, which is larger than that of the other four stations, of which the average proportion of shipping emissions in case L1 reaches 5%, and the
350 average proportion of industrial emissions and residential emissions is smaller than that of the other four stations. WELBZ is located in Chancheng District, which has a complex transportation network, and the average proportion of traffic emissions is 10.1%, which is larger than that of HJC (9.4%). Case L3 and Case L4 found that the average proportion of regional transmission between the five sites was between 96% and 99.4%, and regional transmission was the primary reason for the occurrence of these two
355 cases.





360 **Figure 9: The traceability of NO₂ in the four cases of 5 representative air quality monitoring stations.(a): The traceability of NO₂ in the four cases of HJC (urban-developing station).(b): The traceability of NO₂ in the four cases of HCZZ (urban-developed station).(c): The traceability of NO₂ in the four cases of JJJ(industrial station).(d): The traceability of NO₂ in the four cases of SSYDH(suburban station).(e): The traceability of NO₂ in the four cases of WHLBZ(roadside station).**

4 Discussions and recommendation

4.1 Parameterization mechanism need improvement

365 The urban canopy data used in the WRF model has always had a single representation and ambiguous parameters for the Pearl River Delta region, and the urban canopy is an important factor affecting the wind field simulation and surface energy balance of the urban underlying surface(Chen et al., 2011). Foshan is an important part of the Pearl River Delta urban agglomeration with a high degree of urbanization, and it is expected that the use of refined urban canopy parameters(Chen et al., 2021) to localize the improvement of Foshan's urban structure in the WRF model and update the height and proportion of urban buildings will definitely optimize the meteorological simulation of Foshan by the
370 WRF model.

The complex urban structure (building form, roads, green space, etc.) of Foshan has changed the physical parameters of the underlying surface (such as albedo, specific heat capacity, thermal emissivity, etc.), and the rapid urbanization process of Foshan has had a complex and drastic impact on the land-atmosphere exchange process, thus changing the diffusion conditions and chemical reaction
375 conditions of air pollutants in the city. The chemical mechanism in the EMEP model is EmChem09, which was developed and perfected between 2008 and 2009(Simpson, 2014), but the photochemical reaction module contained in it is simple and difficult to reflect the complex chemical reaction conditions in Foshan. This makes the EMEP model have certain limitations for the simulation of secondary pollutants.

380 4.2 Local emission source and reallocation mechanism need update

The use of China's 2017 monthly average multi-resolution emissions inventory (MEIC) data (27km×27km) to replace the European emission source data in EMEP still has some imprecision in the spatial distribution, although the calculation method mapped to the high-resolution grid is used to ensure that the local emission characteristics remain unchanged after the inventory is replaced, for
385 example, the list of industrial sectors in the inventory does not include enterprises below designated size (industrial enterprises with main business income of less than 20 million yuan) , causing the simulation to fall below the observed threshold. At the same time, the road traffic emissions obtained from OSM do not take into account city-specific traffic congestion or other possible spatial characteristics, and the emissions of enterprises below designated size are also not included in the industrial point source data
390 of Foshan. Therefore, the optimization of possible emission inventories can improve the simulation performance of the EMEP model in high-industrial density megacities to a certain extent, so as to further optimize the simulation performance of the uEMEP model.



5 Conclusion

395 In the past, the air quality forecast of Foshan mainly focused on the prediction and simulation of various
air pollutant concentrations at the mesoscale, without considering the impact of urban structure diversity
on the dispersion of local pollutants. In this study, a high-precision air quality model system was built in
Foshan based on the uEMEP model method, and the application of the block-scale air quality model in
Foshan City, a megacity with high-density industrial development, was realized.

400 The study used meteorological and air quality data to evaluate model performance, classify four
pollution cases, and analyze their spatial characteristics and nitrogen dioxide traceability. The results
show that the uEMEP model can well simulate the distribution of air pollutants at the block scale,
providing insights for targeted air pollution control measures.

405 Air Quality Simulation Performance The European Monitoring and Evaluation Programme (EMEP) and
its City Scale Counterpart Programme (uEMEP) have demonstrated varying degrees of success in
different pollutants and cases. It is worth noting that the uEMEP model performs well in simulating
NO₂ and O₃ in a variety of scenarios, surpassing EMEP in terms of spatial resolution and correlation
with observed data, but the overall deviation is large and needs further improvement.

410 Every pollution event is affected by a combination of meteorological factors and pollution emissions.
The spatial distribution of NO₂ closely follows the distribution of urban road networks, and industrial
emissions significantly affect the spatial pattern of pollutants, highlighting the intertwined relationship
between human activities and air quality.

415 Through a detailed analysis of the traceability characteristics of NO₂ in Foshan, the impacts of regional
transportation, transportation, and industrial emissions on different monitoring stations were revealed. It
is clear that urban center suffer from a complex emission profile, while suburbs may be more vulnerable
to shipping activities.

420 Refining the urban canopy parameters of the WRF model to reflect Foshan's unique urbanization
process can enhance the meteorological simulation. Incorporating emissions from small businesses and
taking into account city-specific traffic attributes can improve the simulation accuracy of EMEP and
uEMEP models. Optimizing emissions inventories is essential to better reflect air quality in
industrialized, densely populated urban areas. In conclusion, multi-scale air quality models are an
indispensable tool for us to interpret the complex dynamics of urban air pollution. Through careful
evaluation and continuous improvement, they lead us towards cleaner and healthier urban
environments.



425 **Code and data availability**

The uEMEP_v6 model used in this study is archived on Zenodo
<https://doi.org/10.5281/zenodo.10708389>(Yang Liting, 2024a).The latest development of uEMEP_v5
model can be downloaded at <https://github.com/metno/uEMEP> (last access: 8 January 2024, Norwegian
Meteorological Institute). The EMEP model version rv4.33 used in this study can be found at
430 <https://github.com/metno/emep-ctm> (last access: 8 January 2024, Norwegian Meteorological Institute).
The configuration file of the EMEP model is archived at
<https://doi.org/10.5281/zenodo.10703324>(Yang Liting, 2024b), as are MATLAB scripts for
visualisation is archived at <https://doi.org/10.5281/zenodo.10714310>(Yang Liting, 2024c).The codes
and datasets in this publication are available to the community, and they can be accessed by request to
435 the corresponding author.

Author contributions: LY (Writing – original draft preparation), MC (Conceptualization,
Methodology), SS (Data curation, Resources), WW (Writing – review & editing), XW (Supervision,
Project administration)

440 **Competing interests:** The authors declare that they have no conflict of interest.

Acknowledgements: This work was supported by the National Natural Science Foundation (42275107,
42230701, 42121004, 41705123), the national Key Research and Development Program of China
(2023YFC3706202), the Science and Technology Projects in Guangzhou (2023A04J0251), the Special
Fund Project for Science and Technology Innovation Strategy of Guangdong Province (Grant
445 No.2019B121205004). The authors thank the High-performance computing platform of Jinan
University, the Research Center of Low Carbon Economy for Guangzhou Region of Jinan University
for their guidance. Road network map data are copyrighted by OpenStreetMap contributors and
available from <https://www.openstreetmap.org> (last access: 23 February 2024).



Appendix A

450 In order to verify the simulation ability and reliability of the model, the observed data and the simulated
 data were used to compare and verify. The deviation (*MB*), mean absolute error (*MAE*), root mean
 square error (*RMSE*), standardized mean deviation (*NMB*) and standardized mean error (*NME*) were
 used to reflect the deviation between the simulated value and the observed value, and the correlation
 455 value and the observed value. *MB*, *MAE*, *RMSE*, *NMB* and *NME* are dimensionally statistical, while *R*
 and *IOA* are dimensionless statistics. In this study, the following criteria were used to judge the
 performance of meteorological condition simulation (Emery and Tai, 2001; Tesche et al., 2002), with
MB ≤ ±0.5K and *IOA* ≥ 0.8 for 2m temperature, *MB* ≤ ±1 g kg⁻¹ and *IOA* ≥ 0.6 for humidity, and *MB* ≤ ±0.5 m
 s⁻¹, *RMSE* ≤ 2.0 m s⁻¹ and *IOA* ≥ 0.6 for 10m wind speed. The evaluation criteria for NO₂ simulation were
 460 -40% < *NMB* < 50%, *NME* < 80%, *R* > 0.3; for O₃ simulation, -15% *NMB* < 15%, *NME* < 35%, *R* > 0.4 ; for
 PM_{2.5} simulation, -50% < *NMB* < 80%, *NME* < 150%, *R* > 0.3.

The specific formula for calculating the above statistics is as follows Eq. (3)-Eq. (9):

$$MB = \frac{1}{N} \sum_{i=1}^N (SIM_i - OBS_i) \quad (3)$$

$$MAE = \frac{1}{N} \sum_{i=1}^N |SIM_i - OBS_i| \quad (4)$$

$$465 \quad RMSE = \sqrt{\frac{1}{N} \sum_{i=1}^N (SIM_i - OBS_i)^2} \quad (5)$$

$$NMB = \frac{\sum_{i=1}^N (SIM_i - OBS_i)}{\sum_{i=1}^N (OBS_i)} \times 100 \quad (6)$$

$$NME = \frac{\sum_{i=1}^N |SIM_i - OBS_i|}{\sum_{i=1}^N (OBS_i)} \times 100 \quad (7)$$

$$R = \frac{\sum_{i=1}^N (SIM_i - \overline{SIM})(OBS_i - \overline{OBS})}{\sqrt{\sum_{i=1}^N (SIM_i - \overline{SIM})^2} \sqrt{\sum_{i=1}^N (OBS_i - \overline{OBS})^2}} \quad (8)$$

$$IOA = 1 - \left[\frac{n \cdot RMSE^2}{\sum_{i=1}^n (|SIM_i| + |OBS_i|)^2} \right] \quad (9)$$

470 where $i=1,2,\dots,N$; N is the length of the sequence; SIM_i and OBS_i are the average values of the
 simulation and observation data; and is the average value of the simulation and observation data, which
 is calculated by the formula $\overline{SIM} = \frac{\sum_{i=1}^N SIM_i}{N}$ and $\overline{OBS} = \frac{\sum_{i=1}^N OBS_i}{N}$.



Appendix B

Table B1: Verification of meteorological factors of WRF model in 4 cases.

Case number	Meteorological factors	<i>OBS</i>	<i>SIM</i>	<i>MB</i>	<i>MAE</i>	<i>RMSE</i>	<i>R</i>	<i>IOA</i>
L1	Temperature(°C)	13.9	14.3	0.4	3.2	3.8	0.8	0.9
	Relative Humidity(%)	55.9	38.7	-17.2	23.6	28.0	0.5	0.6
	Pressure(hPa)	1008.1	1007.0	-1.1	8.8	8.8	0.9	0.9
	Wind Speed(m s ⁻¹)	1.5	2.0	0.6	1.4	1.8	0.4	1.0
L2	Temperature(°C)	15.7	16.3	0.6	2.2	2.7	0.8	0.9
	Relative Humidity(%)	61.4	55.7	-5.7	14.7	18.1	0.7	0.5
	Pressure(hPa)	1008.9	1007.4	-1.6	8.6	8.7	0.9	0.8
	Wind Speed(m s ⁻¹)	1.4	2.4	1.0	1.7	1.9	0.2	0.9
L3	Temperature(°C)	19.2	19.2	0.0	2.3	2.7	0.7	0.9
	Relative Humidity(%)	74.4	68.2	-6.2	12.2	14.6	0.8	0.4
	Pressure(hPa)	1011.5	1010.4	-1.1	8.6	8.7	0.7	0.6
	Wind Speed(m s ⁻¹)	1.3	2.4	1.1	1.7	2.0	0.1	0.9
L4	Temperature(°C)	19.2	19.8	0.5	2.5	2.8	0.7	0.8
	Relative Humidity(%)	84.8	75.5	-9.3	13.1	15.0	0.8	0.1
	Pressure(hPa)	1006.5	1005.1	-1.4	8.5	8.6	0.8	0.6
	Wind Speed(m s ⁻¹)	1.3	2.3	1.0	1.6	1.8	0.1	0.9

475

Table B2: The EMEP and uEMEP models simulate NO₂ performance.

Case number	NO ₂ (µg/m ³)	EMEP	uEMEP
L1	<i>OBS</i>		141.3
	<i>SIM</i>	54.1	54.6
	<i>MB</i>	-88.0	-87.1
	<i>NMB</i>	-60.5	-59.3
	<i>NME</i>	61.3	60.9
	<i>R</i>	0.3	0.2
L2	<i>OBS</i>		119.4
	<i>SIM</i>	49.8	51.2
	<i>MB</i>	-70.2	-68.7
	<i>NMB</i>	-57.9	-56.8
	<i>NME</i>	58.7	58.2
	<i>R</i>	0.6	0.5
L3	<i>OBS</i>		96.7
	<i>SIM</i>	49.5	13.3
	<i>MB</i>	-47.6	-83.4
	<i>NMB</i>	-46.9	-85.0
	<i>NME</i>	53.7	85.3



	<i>R</i>	0.3	-0.2
L4	<i>OBS</i>		92.5
	<i>SIM</i>	34.0	5.0
	<i>MB</i>	-58.9	-87.5
	<i>NMB</i>	-59.8	-90.5
	<i>NME</i>	60.7	90.5
	<i>R</i>	0.5	0.6

Table B3: The EMEP and uEMEP models simulate O₃ performance.

Case number	O ₃ (µg/m ³)	EMEP	uEMEP
L1	<i>OBS</i>		48.6
	<i>SIM</i>	27.1	21.3
	<i>MB</i>	-21.8	-27.5
	<i>NMB</i>	-41.1	-53.8
	<i>NME</i>	69.2	65.8
	<i>R</i>	0.8	0.8
	L2	<i>OBS</i>	
<i>SIM</i>		25.7	21.2
<i>MB</i>		-14.7	-19.1
<i>NMB</i>		-32.6	-44.9
<i>NME</i>		63.9	61.8
<i>R</i>		0.8	0.8
L3		<i>OBS</i>	
	<i>SIM</i>	24.9	50.4
	<i>MB</i>	-39.3	-13.9
	<i>NMB</i>	-60.6	-19.5
	<i>NME</i>	74.9	75.7
	<i>R</i>	0.6	0.9
	L4	<i>OBS</i>	
<i>SIM</i>		33.7	53.8
<i>MB</i>		-6.9	13.1
<i>NMB</i>		-13.7	38.0
<i>NME</i>		56.1	70.3
<i>R</i>		0.7	0.8

480

Table B4: The EMEP and uEMEP models simulate PM_{2.5} performance.

Case number	PM _{2.5} (µg/m ³)	EMEP	uEMEP
L1	<i>OBS</i>		106.9
	<i>SIM</i>	24.3	27.0
	<i>MB</i>	-83.0	-80.0
	<i>NMB</i>	-76.4	-73.4



	<i>NME</i>	76.4	73.6
	<i>R</i>	0.4	0.2
L2	<i>OBS</i>		82.9
	<i>SIM</i>	20.7	25.4
	<i>MB</i>	-62.6	-57.7
	<i>NMB</i>	-74.9	-69.0
	<i>NME</i>	74.9	69.0
	<i>R</i>	0.5	0.3
L3	<i>OBS</i>		70.4
	<i>SIM</i>	21.0	9.9
	<i>MB</i>	-49.6	-60.6
	<i>NMB</i>	-69.2	-85.2
	<i>NME</i>	69.6	85.2
	<i>R</i>	0.2	0.0
L4	<i>OBS</i>		71.2
	<i>SIM</i>	14.3	5.5
	<i>MB</i>	-57.2	-65.9
	<i>NMB</i>	-76.0	-88.3
	<i>NME</i>	76.1	88.3
	<i>R</i>	0.2	0.3

485 **Table B5: The EMEP and uEMEP models simulate PM₁₀ performance.**

Case number	PM ₁₀ (µg/m ³)	EMEP	uEMEP
L1	<i>OBS</i>		181.5
	<i>SIM</i>	51.2	41.8
	<i>MB</i>	-131.1	-140.0
	<i>NMB</i>	-71.0	-75.8
	<i>NME</i>	71.2	76.0
	<i>R</i>	0.3	0.1
L2	<i>OBS</i>		163.9
	<i>SIM</i>	42.6	40.0
	<i>MB</i>	-121.9	-124.3
	<i>NMB</i>	-74.0	-75.6
	<i>NME</i>	74.0	75.6
	<i>R</i>	0.4	0.3
L3	<i>OBS</i>		131.4
	<i>SIM</i>	43.7	14.4
	<i>MB</i>	-88.1	-117.1
	<i>NMB</i>	-66.2	-88.6
	<i>NME</i>	66.6	88.6
	<i>R</i>	0.2	0.0
L4	<i>OBS</i>		116.8
	<i>SIM</i>	31.3	8.4
	<i>MB</i>	-86.5	-109.0
	<i>NMB</i>	-70.4	-89.3
	<i>NME</i>	71.9	89.8
	<i>R</i>	0.4	0.4



References

- Anjali, S. and Rao, B. P. S.: Urban Air Pollution Modeling, 10.5772/16776, 2011.
- 490 Bai, H., Song, J., Wu, H., Yan, R., Gao, W., and Hussain, M. J.: Assessment of personal exposure using movement trajectory and hourly 1-km PM_{2.5} concentrations, 18 %J Journal of Applied Remote Sensing, 012003, 2023.
- Baklanov, A. and Nuterman, R.: Multi-scale atmospheric environment modelling for urban areas, *Advances in Science and Research*, 3, 53-57, 10.5194/asr-3-53-2009, 2009.
- Beevers, S., Kitwiroon, N., Williams, M., and Carslaw, D.: One way coupling of CMAQ and a road source dispersion model for fine scale air pollution predictions, *Atmospheric Environment*, 59, 47-58, 10.1016/j.atmosenv.2012.05.034, 2012.
- 495 Bo, T., Deguan, C., Hao, L., Weixing, X., and Lin, L.: Spatial evolution and influencing factors of Foshan's high-tech industry under the background of high-quality development, *World Regional Studies*, 32, 2023.
- Chen, B., Wang, W., Dai, W., Chang, M., Wang, X., You, Y., Zhu, W., and Liao, C.: Refined urban canopy parameters and their impacts on simulation of urbanization-induced climate change, *Urban Climate*, 37, 10.1016/j.uclim.2021.100847, 2021.
- 500 Chen, F., Hiroyuki, K., Robert, B., Jason, C., B., G. C. S., Susanne, G.-C., Thomas, L., W., M. K., Alberto, M., Shiguang, M., David, S., P., S. F., Haider, T., Mukul, T., Xuemei, W., A., W. A., and Chaolin, Z.: The integrated WRF/urban modelling system: development, evaluation, and applications to urban environmental problems, *International Journal of Climatology*, 31, 273-288, <https://doi.org/10.1002/joc.2158>, 2011.
- Criado, A., Mateu Armengol, J., Petetin, H., Rodríguez-Rey, D., Benavides, J., Guevara, M., Pérez García-Pando, C., Soret, A., and Jorba, O.: Data fusion uncertainty-enabled methods to map street-scale hourly
- 505 NO₂ in Barcelona city: a case study with CALIOPE-Urban v1.0, 10.5194/egusphere-2022-1147, 2022.
- Denby, B., Gauss, M., Wind, P., Mu, Q., Wærsted, E., Fagerli, H., Valdebenito, A., and Klein, H.: Description of the uEMEP_v5 downscaling approach for the EMEP MSC-W chemistry transport model, *Geoscientific Model Development*, 13, 6303-6323, 10.5194/gmd-13-6303-2020, 2020.
- Ecological and Environmental Monitoring Centre of Guangdong, Environmental Protection Department, H. K. S., , ,
- 510 Environmental Protection Bureau, M. S., , and Environmental Protection Bureau, M. S.: The statistical summary of the monitoring results of the PRD Regional Air Quality Monitoring Network in April to June, the second quarter of 2023, PRDAIR-2023-2, <https://gdee.gd.gov.cn/attachment/0/536/536771/4272990.pdf>, 2023.
- Emery, C. and Tai, E.: Enhanced Meteorological Modeling and Performance Evaluation for Two Texas Ozone Episodes, Foshan Emergency Management Bureau and Office, F. C. S. P. C.: Foshan City's 2021 safety training and education action
- 515 plan for resumption of production and work after the holidays, <https://fscm.foshan.gov.cn/attachment/0/175/175228/4768228.pdf>, 2021.
- Gavidia-Calderón, M. E., Ibarra-Espinosa, S., Kim, Y., Zhang, Y., and Andrade, M. d. F.: Simulation of O₃ and NO_x in São Paulo street urban canyons with VEIN (v0.2.2) and MUNICH (v1.0), *Geoscientific Model Development*, 14, 3251-3268, 10.5194/gmd-14-3251-2021, 2021.
- 520 Isakov, V., Arunachalam, S., Baldauf, R., Breen, M., Deshmukh, P., Hawkins, A., Kimbrough, S., Krabbe, S., Naess, B., Serre, M., and Valencia, A.: Combining Dispersion Modeling and Monitoring Data for Community-Scale Air Quality Characterization, *Atmosphere*, 10, 610, 10.3390/atmos10100610, 2019.
- Kim, Y., Wu, Y., Seigneur, C., and Roustan, Y.: Multi-scale modeling of urban air pollution: development and application of a Street-in-Grid model (v1.0) by coupling MUNICH (v1.0) and Polair3D (v1.8.1), *Geoscientific Model Development*, 11, 611-629, 10.5194/gmd-11-611-2018, 2018.
- 525 Li, Z., Ho, K.-F., Chuang, H.-C., and Yim, S. H. L.: Development and intercity transferability of land-use regression models for predicting ambient PM₁₀, PM_{2.5}, NO₂ and O₃ concentrations in northern Taiwan, *Atmospheric Chemistry and Physics*, 21, 5063-5078, 10.5194/acp-21-5063-2021, 2021.
- Li, Z., Ho, K.-F., Lee, H. F., and Yim, S. H. L.: Development of an integrated model framework for multi-airpollutant
- 530 exposure assessments in high-density cities and the implications for epidemiological research, 10.5194/egusphere-2023-513, 2023.
- Liu, W., Shen, J., and Wei, Y.: Spatial restructuring of pollution-intensive enterprises in Foshan China: Effects of the changing role of environmental regulation, *Journal of Environmental Management*, 325, 10.1016/j.jenvman.2022.116501, 2023.



- 535 Liu, Y., Yu, Z., Huang, Y., Cai, M., Xu, W., and Li, L.: Analysis of uneven distribution characteristics of urban air pollution, *China Environmental Monitoring*, 27, 2011.
- Maciej Kryza, M. W., Bruce Rolstad Denby, Qing Mu, Tymoteusz Sawiński & Arkadiusz Remut Forecasting PM2.5 Concentrations with uEMEP and EMEP4PL for Poland, *Air Pollution Modeling and its Application XXVIII2022*.
- 540 Mu, Q., Denby, B., Wærsted, E., and Fagerli, H.: Downscaling of air pollutants in Europe using uEMEP_v6, *Geoscientific Model Development*, 15, 449-465, 10.5194/gmd-15-449-2022, 2022.
- OpenStreetMap contributors: Planet dump retrieved from <https://planet.osm.org/>, available at: <https://www.openstreetmap.org> (last access: 23 February 2024), 2020.
- Parvez, F. and Wagstrom, K.: A hybrid modeling framework to estimate pollutant concentrations and exposures in near road environments, *Science of The Total Environment*, 663, 144-153, <https://doi.org/10.1016/j.scitotenv.2019.01.218>, 2019.
- 545 Russo, M., Gama, C., and Monteiro, A.: How does upgrading an emissions inventory affect air quality simulations?, *Air Quality Atmosphere and Health*, 12, 731-741, 10.1007/s11869-019-00692-x, 2019.
- Silveira, C., Ferreira, J., and Miranda, A.: A multiscale air quality and health risk modelling system: Design and application over a local traffic management case study, *Atmospheric Environment*, 294, 10.1016/j.atmosenv.2022.119481, 2023.
- Simpson, D.: The EMEP MSC-W Modelling Programme: Its Relationship to Policy Support, Current Challenges and Future Perspectives, *Air Pollution Modeling and its Application XXII2014*.
- 550 Simpson, D., Benedictow, A., Berge, H., Bergström, R., Emberson, L. D., Fagerli, H., Flechard, C. R., Hayman, G. D., Gauss, M., Jonson, J. E., Jenkin, M. E., Nyíri, A., Richter, C., Semeena, V. S., Tsyro, S., Tuovinen, J. P., Valdebenito, Á., and Wind, P.: The EMEP MSC-W chemical transport model – technical description, *Atmospheric Chemistry and Physics*, 12, 7825-7865, 10.5194/acp-12-7825-2012, 2012.
- 555 Tesche, T., McNally, D. E., and Tremback, C. J.: Draft Protocol OPERATIONAL EVALUATION OF THE MM 5 METEOROLOGICAL MODEL OVER THE CONTINENTAL UNITED STATES : Protocol for Annual and Episodic Evaluation Task Order 4 TCG-68027015,
- Weger, M. and Heinold, B.: Air pollution trapping in the Dresden Basin from gray-zone scale urban modeling, *Atmospheric Chemistry and Physics*, 23, 13769-13790, 10.5194/acp-23-13769-2023, 2023.
- 560 Whaley, C. H., Galarneau, E., Makar, P. A., Moran, M. D., and Zhang, J.: How much does traffic contribute to benzene and polycyclic aromatic hydrocarbon air pollution? Results from a high-resolution North American air quality model centred on Toronto, Canada, *Atmospheric Chemistry and Physics*, 20, 2911-2925, 10.5194/acp-20-2911-2020, 2020.
- Yan, F. H., Chen, W. H., Chang, M., Wang, W. W., Liu, Y. L., Zhong, B. Q., Mao, J. Y., Yang, T. S., Wang, X. M., and Liu, C. F.: [Characteristics and Meteorological Factors of Complex Nonattainment Pollution of Atmospheric Photochemical Oxidant (O₃), *Huan Jing Ke Xue*, 42, 1600-1614, 10.13227/j.hj.kx.202007286, 2021.
- 565 Yang Liting: uEMEP model file for the study "Development And Application of WRF(v4.1.2)-uEMEP(v5) Model at the City with the Highest Industrial Density: A Case Study of Foshan" [dataset], 10.5281/zenodo.10708389, 2024a.
- Yang Liting: EMEP model configuration file for the study "Development And Application of WRF(v4.1.2)-uEMEP(v5) Model at the City with the Highest Industrial Density: A Case Study of Foshan" [dataset], 10.5281/zenodo.10703324, 2024b.
- 570 Yang Liting: EMEP and uEMEP matlab plotting scripts for visualisation [dataset], 10.5281/zenodo.10714310, 2024c.